Available online at www.sciencedirect.com
ScienceDirect
Applied Mathematics and Computation 197 (2008) 426–434
APPLIED MATHEMATICS AND COMPUTATION
www.elsevier.com/locate/amc

Numerical meshfree path integration method for non-linear dynamic systems ☆

Wen-Xian Xie [a,*], Wei Xu [a], Li Cai [b]

[a] School of Science, Northwestern Polytechnical University, Xi'an, Shaanxi 710072, China
[b] College of Astronautics, Northwestern Polytechnical University, Xi'an, Shaanxi 710072, China

Abstract

We present a new numerical meshfree path integration (MPI) method for non-linear dynamic systems. The obtained MPI method can be performed in the irregular computational domain and the probability density values of the random nodes in the domain can be calculated via the MPI method and the ordinary differential equations for the first and second-order moments on the basis of Gaussian closure method. The piecewise linear interpolation based on adaptive least squares is utilized as a post processor to approximate the probability density values on arbitrary positions. The good performance of the resulting method is finally shown in the numerical examples by using three specific non-linear dynamic systems: Duffing oscillator subjected to both harmonic and stochastic excitations, Duffing–Rayleigh oscillator subjected to both harmonic and stochastic excitations, and CHEN system driven by three different Gaussian white noises.

Keywords: Path integration method; Meshfree method; Non-linear dynamic systems

1. Introduction

Path integration has been used to give formal solutions to Fokker–Planck–Kolmogorov (FPK) equation with time-independent and explicitly time-dependent drift and diffusion coefficients [1]. The key issue in the path integration method is the observation that an approximate solution of FPK equation can be represented as a product of short-time transition probability densities and the Markov response process can locally be approximated by a Gaussian diffusion [2–13].

Every existing path integration procedure employs a certain integration scheme in which the probability density is represented by its values at discrete grid points. Among the first systematic efforts to develop the path integration method into a numerical tool are those of Wehner and Wolfer [2–4] and the piecewise constant interpolation scheme used in their papers. The general results in lower values near the peaks and higher values at the tails.

☆ Project supported by the National Natural Science Foundation of China (Grant Nos. 10472091 and 10332030).
* Corresponding author.
E-mail addresses: wenxianxie@nwpu.edu.cn (W.-X. Xie), eign@eyou.com (L. Cai).

0096-3003/$ - see front matter
doi:10.1016/j.amc.2007.07.088

Nasess and Johnsen [5] showed that the path integration method could be implemented in such a manner that extremely accurate results could be obtained for the tail behavior of the joint probability density of the state space vector of both 2D and 3D cases. This makes the path integration method of particular interest for the estimation of extreme responses of dynamical systems which can be modelled as non-linear oscillator excited by forces, external or parametric, that can be approximated as white noise or filtered white noise processes [5–7]. The interpolation by cubic B-spline function has been used to gain a satisfactory probability density accurate to the order 10^{-6} at the tails [8]. However, the computational time for spline interpolation increases exponentially with the number of dimension.

A different procedure for path integration is proposed on the basis of the Gauss–Legendre integration scheme, which is equivalent to replacing the function to the integrated directly with an interpolation polynomial of the certain order [9] and has been applied to a Duffing oscillator subject to both sinusoidal and white noise excitations [10]. The capability of capturing the evolution of the probability density for the non-homogeneous Markov process is elaborated in details. The simplicity and efficiency of the procedure is remarkable among all path integration method in present.

Path integration, an approach to solving FPK equation is more natural numerical method and powerful for capture the evolution of probability density. The numerical implementation of the above technique consists in using the Chapman–Smoluchowski equation to follow the time evolution of the process through small elementary steps and then employing the appropriate interpolation procedures. The application of the method to higher-dimensional systems seems to be difficult, the example elaborated in the existing literature, known to the authors of this paper, are concerned with non-linear oscillators.

In the following sections, we will derive the MPI method and show how the method can be used to capture the evolution of probability density of the complex stochastic dynamical system whether the deterministic system is chaotic or periodic.

2. Meshfree path integration method

The derivation of the MPI method is straightforward. The idea of original path integration is to compute the long-term transition of probability distribution in small steps and the computation can be performed in a reduced finite range, Ω_r, in the state space Ω. This finite range is so determined that the probability values outside the range is sufficiently low that its effect can be neglected. We can express a typical evolution of a probability density $p(\mathbf{x}, t)$ from time t_{n-1} to t_n as follows:

$$p^n(\mathbf{x}) := p(\mathbf{x}, t_n) = \int_{\Omega_r} q(\mathbf{x}, t_n|\tilde{\mathbf{x}}, t_{n-1}) p(\tilde{\mathbf{x}}, t_{n-1}) \mathrm{d}\tilde{\mathbf{x}}. \tag{2.1}$$

The essential features of the MPI algorithm will be illustrated herein. We suppose that we scatter the computational domain Ω_r randomly with N nodes $\{\mathbf{x}_s\}_{s=1}^N$. Then Ω_r can be tessellated by N polygonal (for 2D systems) or polyhedral (for 3D systems) sub-domain Ω_s $(s = 1, \ldots, N)$ and keep each $\mathbf{x}_s$ as the center of Ω_s (i.e., $\mathbf{x}_s := (L_1^s, \ldots, L_p^s) = (1/p, \ldots, 1/p)$, where p is the nodes number of the polygon (or polyhedron) Ω_s and L_j^s $(j = 1, \ldots, p)$ are the area (or volume) coordinates of the polygon (or polyhedron) Ω_s). In this case, the integral (2.1) can be discretized into the following composite quadrature form

$$p^n(\mathbf{x}_j) = \sum_{s=1}^{N} [S_{\Omega_s} q(\mathbf{x}_j, t_n|\tilde{\mathbf{x}}_s, t_{n-1}) p^{n-1}(\tilde{\mathbf{x}}_s)] + \mathcal{O}(h^2) \quad (j = 1, \ldots, N). \tag{2.2}$$

Here S_{Ω_s} is the area (or volume) of Ω_s and h is the minimum characteristic size of all sub-domain Ω_s.

Without loss of generality, we let N sub-domain Ω_s $(s = 1, \ldots, N)$ are triangulations (for 2D systems) or tetrahedrons (for 3D systems). Obviously, reduction to one dimension, extension to higher dimensions and applications to other unstructured and structured meshes are all straightforward variations on the theme.

3. Piecewise linear interpolation based on adaptive least squares

Now, we describe the piecewise linear interpolation that we have used in our numerical experiments as a post processor to approximate the probability density values on arbitrary positions in the computational domain.

Consider the 2D piecewise linear interpolation $R^n(x,y)$ on a triangular cell Δ_l, i.e. $p_l^n(x,y)$. Conservation of the mean within Δ_l requires that $\int_{\Delta_l} p_l^n(x,y)\mathrm{d}x\,\mathrm{d}y = \int_{\Delta_l} u^n(x,y)\mathrm{d}x\,\mathrm{d}y$, and this can be accomplished by using zero-mean polynomials in expanding about the center of mass, $\mathbf{x}_l = (x_l, y_l)$, see Fig. 1,

$$p_l^n(x,y) = \bar{u}_l^n + \left.\frac{\partial u}{\partial x}\right|_l^n (x - x_l - \bar{x}_l) + \left.\frac{\partial u}{\partial y}\right|_l^n (y - y_l - \bar{y}_l), \tag{3.3}$$

where $\bar{x}_l = \frac{1}{|\Delta_l|}\int_{\Delta_l}(x - x_l)\mathrm{d}x\,\mathrm{d}y$ and $\bar{y}_l = \frac{1}{|\Delta_l|}\int_{\Delta_l}(y - y_l)\mathrm{d}x\,\mathrm{d}y$. We apply three equations $\frac{1}{|\Delta_m|}\int_{\Delta_m} p_l^n(x,y)\mathrm{d}x\,\mathrm{d}y = \bar{u}_m^n$ $(m = i,j,k)$ to estimate the coefficients $\left.\frac{\partial u}{\partial x}\right|_l^n$ and $\left.\frac{\partial u}{\partial y}\right|_l^n$. The mean value, for a single cell Δ_m, of the reconstructed polynomial $p_l^n(x,y)$ is

$$\begin{aligned}\frac{1}{|\Delta_m|}\int_{\Delta_m} p_l^n(x,y)\mathrm{d}x\,\mathrm{d}y &= \bar{u}_l^n + \left.\frac{\partial u}{\partial x}\right|_l^n \left(\frac{1}{|\Delta_m|}\int_{\Delta_m}(x - x_l)\mathrm{d}x\,\mathrm{d}y - \bar{x}_l\right) \\ &\quad + \left.\frac{\partial u}{\partial y}\right|_l^n \left(\frac{1}{|\Delta_m|}\int_{\Delta_m}(y - y_l)\mathrm{d}x\,\mathrm{d}y - \bar{y}_l\right) \\ &= \bar{u}_l^n + \left.\frac{\partial u}{\partial x}\right|_l^n (\bar{x}_m + (x_m - x_l) - \bar{x}_l) + \left.\frac{\partial u}{\partial y}\right|_l^n (\bar{y}_m + (y_m - y_l) - \bar{y}_l).\end{aligned} \tag{3.4}$$

Let $\tilde{x}_{lm} = \bar{x}_m + (x_m - x_l) - \bar{x}_l$ and $\tilde{y}_{lm} = \bar{y}_m + (y_m - y_l) - \bar{y}_l$, and then we can easily write down a least squares problem for the derivatives

$$\begin{bmatrix} \tilde{x}_{li} & \tilde{y}_{li} \\ \tilde{x}_{lj} & \tilde{y}_{lj} \\ \tilde{x}_{lk} & \tilde{y}_{lk} \end{bmatrix} \begin{bmatrix} \left.\frac{\partial u}{\partial x}\right|_l^n \\ \left.\frac{\partial u}{\partial y}\right|_l^n \end{bmatrix} = \begin{bmatrix} \bar{u}_i^n - \bar{u}_l^n \\ \bar{u}_j^n - \bar{u}_l^n \\ \bar{u}_k^n - \bar{u}_l^n \end{bmatrix}. \tag{3.5}$$

The solution of the least squares problem is given as

$$\begin{bmatrix} \left.\frac{\partial u}{\partial x}\right|_l^n \\ \left.\frac{\partial u}{\partial y}\right|_l^n \end{bmatrix} = \frac{1}{\sqrt{\sum_{m=i,j,k}\tilde{x}_{lm}^2 \sum_{m=i,j,k}\tilde{y}_{lm}^2 - \left(\sum_{m=i,j,k}\tilde{x}_{lm}\tilde{y}_{lm}\right)^2}} \cdot \begin{bmatrix} \sum_{m=i,j,k}\tilde{y}_{lm}^2 \sum\limits_{m=i,j,k}\tilde{x}_{lm}\tilde{u}_{lm}^n - \sum\limits_{m=i,j,k}\tilde{x}_{lm}\tilde{y}_{lm} \sum\limits_{m=i,j,k}\tilde{y}_{lm}\tilde{u}_{lm}^n \\ \sum\limits_{m=i,j,k}\tilde{x}_{lm}^2 \sum\limits_{m=i,j,k}\tilde{y}_{lm}\tilde{u}_{lm}^n - \sum\limits_{m=i,j,k}\tilde{x}_{lm}\tilde{y}_{lm} \sum\limits_{m=i,j,k}\tilde{x}_{lm}\tilde{u}_{lm}^n \end{bmatrix} \tag{3.6}$$

with $\tilde{u}_{lm}^n = \bar{u}_m^n - \bar{u}_l^n$ $(m = i,j,k)$.

Next, we improve the resolution present in the basic reconstruction (3.3) and (3.6), by searching two most available triangles among Δ_l's three neighboring triangles $\{\Delta_i, \Delta_j, \Delta_k\}$. First we calculate the outer normals of piecewise planes computed from the basic reconstruction (3.3) and (3.6). We then compute the angles between

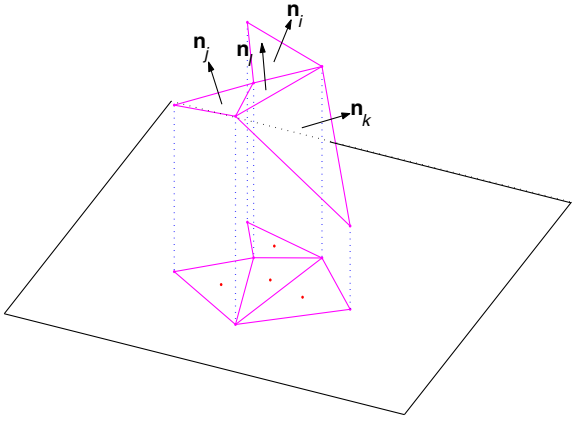

Fig. 1. Stencil-searching.

$\mathbf{n}_l$ and $\mathbf{n}_m$ $(m = i, j, k)$. For example, if the angle between $\mathbf{n}_l$ and $\mathbf{n}_k$ is biggest, we should choose cells Δ_i and Δ_j to determine the two derivatives exactly, illustrated by Fig. 1. Here, the new reconstruction is the so-called piecewise linear interpolation based on adaptive least squares. More details we refer readers to [14]. The 3D piecewise linear interpolation $R^n(x, y, z)$ can be derived in the similar way.

4. Numerical examples

In this section, two specific 2D non-linear dynamic systems, Duffing oscillator and Duffing–Rayleigh oscillator subjected to both harmonic and stochastic excitations, and 3D CHEN systems are solved numerically via the MPI method. The 2D and 3D initial Gaussian distributions are offered as

$$q(\mathbf{x}, 0) = \frac{1}{2\pi|\mathbf{B}|^{1/2}} \exp\left\{-\frac{1}{2}(\mathbf{x} - \mathbf{a_0})^{\mathrm{T}}\mathbf{B}^{-1}(\mathbf{x} - \mathbf{a_0})\right\}, \tag{4.7}$$

where $\mathbf{x} = (x, y)^{\mathrm{T}} \in \Omega_r$, $a_0 = (\mu_1, \mu_2)^{\mathrm{T}}$ and $\mathbf{B} = \begin{bmatrix} s_1^2 & s_1 s_2 r_{12} \\ s_1 s_2 r_{12} & s_2^2 \end{bmatrix}$, and

$$q(\mathbf{x}, 0) = \frac{1}{(2\pi)^{3/2}|\mathbf{B}|^{1/2}} \exp\left\{-\frac{1}{2}(\mathbf{x} - \mathbf{a_0})^{\mathrm{T}}\mathbf{B}^{-1}(\mathbf{x} - \mathbf{a_0})\right\}, \tag{4.8}$$

where $\mathbf{x} = (x, y, z)^{\mathrm{T}} \in \Omega_r$, $a_0 = (\mu_1, \mu_2, \mu_3)^{\mathrm{T}}$ and $\mathbf{B} = \begin{bmatrix} s_1^2 & s_1 s_2 r_{12} & s_1 s_3 r_{13} \\ s_2 s_1 r_{12} & s_2^2 & s_2 s_3 r_{23} \\ s_3 s_1 r_{13} & s_3 s_2 r_{23} & s_3^2 \end{bmatrix}$.

4.1. Duffing oscillator

Firstly, we consider a Duffing oscillator subjected to both sinusoidal and white noise excitations, governed by the following equation of motion:

$$\ddot{x} + \eta\dot{x} + \alpha x + \beta x^3 = F\cos\omega t + \sigma\xi(t), \tag{4.9}$$

where $\xi(t)$ is a Gaussian white noise with unit intensity. The equations for the first- and second-order moments on the basis of Gaussian closure are given by

$$\begin{cases} \dot{m}_{10} = m_{01}, \\ \dot{m}_{01} = -\eta m_{01} - \alpha m_{10} - 3\beta m_{10} m_{20} + 2\beta m_{10}^3 + F\cos\omega t, \\ \dot{m}_{11} = m_{02} - \eta m_{11} - \alpha m_{20} - 3\beta m_{20}^2 + 2\beta m_{10}^4 + m_{10} F\cos\omega t, \\ \dot{m}_{20} = 2m_{11}, \\ \dot{m}_{02} = -2\eta m_{02} - 2\alpha m_{11} - 6\beta m_{20} m_{11} + 4\beta m_{10}^3 m_{01} + \sigma^2 + 2m_{01} F\cos\omega t, \end{cases} \tag{4.10}$$

where $m_{ij} = E[x^i, y^j] = E[x^i, \dot{x}^j]$. Eqs. (4.10) are some time-dependent ODEs, which can be solved by any stable ODE solver which retains the spatial accuracy of the method. In the numerical example below, we have used the fourth-order natural continuous extensions of Runge–Kutta (NCERK) method, proposed in [15].

Therefore, the 2D transitional Gaussian distributions are derived as

$$q(\mathbf{x}, t_n|\tilde{\mathbf{x}}, t_{n-1}) = \frac{1}{2\pi|\mathbf{B}(\tilde{\mathbf{x}}, t_n)|^{1/2}} \exp\left\{-\frac{1}{2}[\mathbf{x} - \mathbf{a}(\tilde{\mathbf{x}}, \mathbf{t_n})]^{\mathrm{T}}\mathbf{B}(\tilde{\mathbf{x}}, t_n)^{-1}[\mathbf{x} - \mathbf{a}(\tilde{\mathbf{x}}, \mathbf{t_n})]\right\}, \tag{4.11}$$

where $\mathbf{x} = (x, y)^{\mathrm{T}}$, $\tilde{\mathbf{x}} = (\tilde{x}, \tilde{y})^{\mathrm{T}}$ and $a_0 = [m_{10}(\tilde{\mathbf{x}}, t_n), m_{01}(\tilde{\mathbf{x}}, t_n)]^{\mathrm{T}}$ and

$$\mathbf{B}(\tilde{\mathbf{x}}, t_n) = \begin{bmatrix} m_{20}(\tilde{\mathbf{x}}, t_n) - [m_{10}(\tilde{\mathbf{x}}, t_n)]^2 & m_{11}(\tilde{\mathbf{x}}, t_n) - m_{10}(\tilde{\mathbf{x}}, t_n) m_{01}(\tilde{\mathbf{x}}, t_n) \\ m_{11}(\tilde{\mathbf{x}}, t_n) - m_{10}(\tilde{\mathbf{x}}, t_n) m_{01}(\tilde{\mathbf{x}}, t_n) & m_{02}(\tilde{\mathbf{x}}, t_n) - [m_{01}(\tilde{\mathbf{x}}, t_n)]^2 \end{bmatrix}.$$

There are 3372 nodes in the square computational domain, $[-4, 4] \times [-4, 4]$, and the time step Δt is $T/4$ (here $T = 2\pi/\omega$). The parameters of the initial Gaussian distribution are $\mu_1 = \mu_2 = -1.0$, $s_1^2 = s_2^2 = 0.1$ and $r_{12} = 0.01$. For computation, we choose the following system and excitation parameters: $\alpha = 1.0$, $\beta = 0.3$, $\eta = 0.1$, $F = 0.2$, $\omega = 1.2$ and $\sigma^2 = 0.01$. Fig. 2 describes the periodic quality of the probability density, which has the good agreement with the reports in Ref. [10].

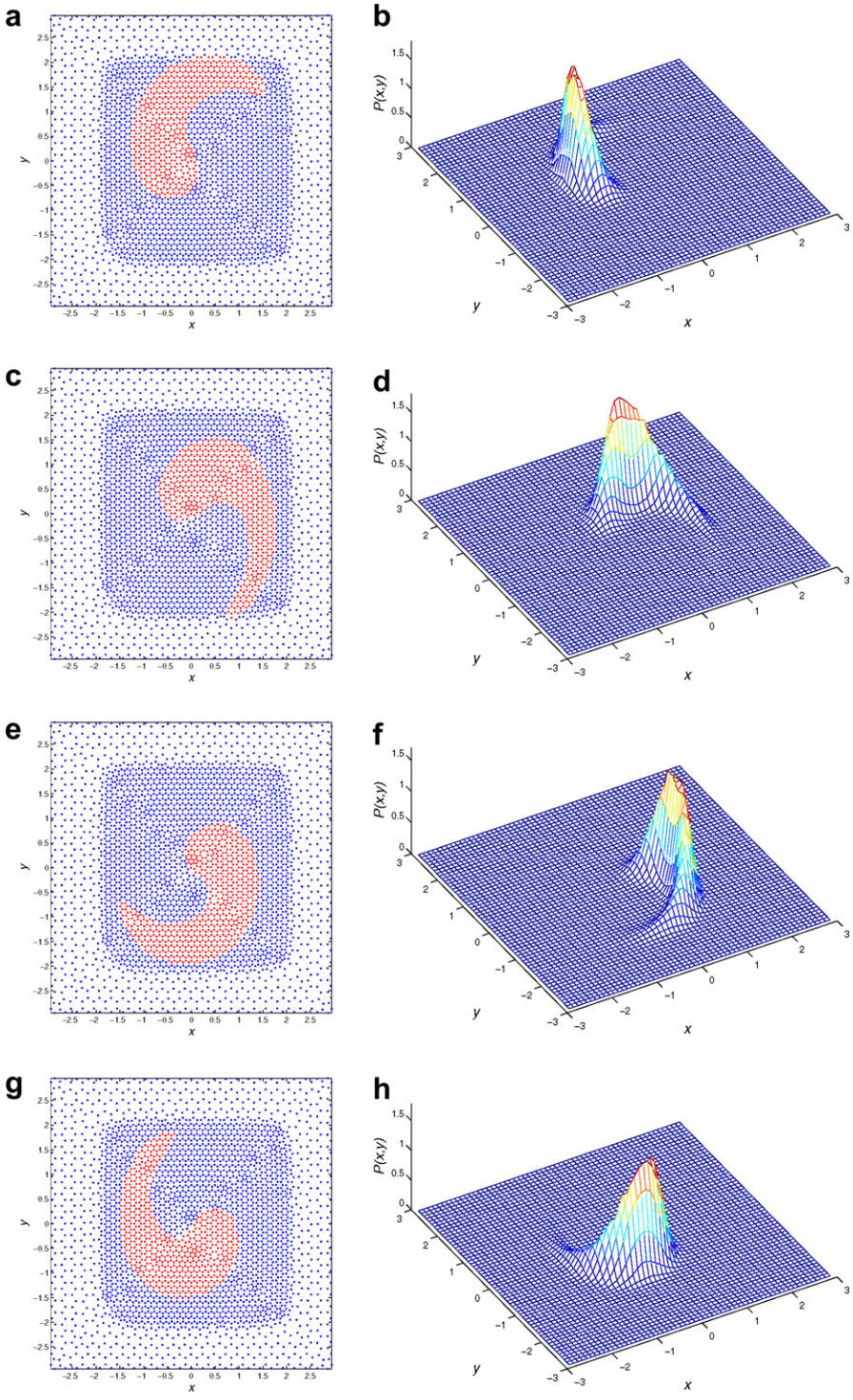

Fig. 2. Numerical results for Duffing oscillator: (a) 2D plots at time $T/4$: red nodes for $P(x,y) > 10^{-3}$, (b) surface plots at time $T/4$, (c) 2D plots at time $T/2$: red nodes for $P(x,y) > 10^{-3}$, (d) surface plots at time $T/2$, (e) 2D plots at time $3T/4$: red nodes for $P(x,y) > 10^{-3}$, (f) surface plots at time $3T/4$, (g) 2D plots at time T: red nodes for $P(x,y) > 10^{-3}$ and (h) surface plots at time T. (For interpretation of the references to color in this figure legend, the reader is referred to the web version of this article.)

4.2. Duffing–Rayleigh oscillator

Then we discuss the Duffing–Rayleigh oscillator subjected to both harmonic and stochastic excitations described by

$$\ddot{x}+\gamma\left(1+\frac{\beta}{\omega_1^2}\dot{x}^2\right)\dot{x}+\omega_1^2(1+\varepsilon x^2)x=\omega_1\sigma_1\sin\omega t+\omega_1\sigma_2\xi(t), \tag{4.12}$$

where ω_1 is the natural circle frequency and γ is the linear damping coefficient. β and ε are the non-linear parameters. σ_1 and ω are intensity and frequency of the harmonic excitation respectively, and σ_2 is the intensity of the additive white noise $\xi(t)$.

The equations for the first- and second-order moments on the basis of Gaussian closure are also given by

$$\begin{cases}
\dot{m}_{10}=m_{01},\\
\dot{m}_{01}=-\frac{\gamma\beta}{\omega_1^2}(3m_{01}m_{02}-2m_{01}^3)-\omega_1^2\varepsilon(3m_{10}m_{20}-2m_{10}^3)-\gamma m_{01}-\omega_1^2m_{10}+\omega_1\sigma_1\sin\omega t,\\
\dot{m}_{11}=m_{02}+\frac{\gamma\beta}{\omega_1^2}(2m_{01}^3m_{10}-3m_{02}m_{11})+\omega_1^2\varepsilon(2m_{01}^4-3m_{20}^2)-\gamma m_{11}-\omega_1^2m_{20}+\omega_1\sigma_1m_{10}\sin\omega t,\\
\dot{m}_{20}=2m_{11},\\
\dot{m}_{02}=\frac{\gamma\beta}{\omega_1^2}(4m_{01}^4-6m_{02}^2)+\omega_1^2\varepsilon(4m_{10}^3m_{01}-6m_{20}m_{11})-2\gamma m_{02}-2\omega_1^2m_{11}+2\omega_1\sigma_1m_{01}\sin\omega t+\omega_1^2\sigma_2^2.
\end{cases} \tag{4.13}$$

Eq. (4.13) are solved by the fourth-order NCERK method.

There are 5496 nodes in the circular computational domain with the radius $r=5$. We choose the time step Δt as $T=2\pi/\omega$. The parameters of the initial Gaussian distribution are $\mu_1=-2,\ \mu_2=-1.8,\ s_1^2=s_2^2=1$ and $r_{12}=0$. Here $\gamma=0.2,\ \beta=0.0,\ \varepsilon=0.3,\ \omega_1=1.0,\ \omega=1.6,\ \sigma_1=1.0,\ \sigma_2=0.4$. Fig. 3 shows the new MPI method is useful to capture the evolutions of the probability density in a long time. Much more numerical experiments are expected to implement by our method to study the behaviors of the probability density.

4.3. CHEN system

In 1999, CHEN found a similar but nonequivalent chaotic attractor from the so-called CHEN system. Recently, the study of the intrinsic dynamics about the CHEN system has evolved further investigation (cf. [16,17] and references therein).

Consider the following CHEN system driven by three different Gaussian white noises

$$\begin{cases}
\dot{x}=a(y-x)+\sigma_1\xi_1(t),\\
\dot{y}=(c-a)x-xz+cy+\sigma_2\xi_2(t),\\
\dot{z}=xy-bz+\sigma_3\xi_3(t),
\end{cases} \tag{4.14}$$

where $\langle\xi_i(t)\rangle=0$ and $\langle\xi_i(t),\xi_j(t')\rangle=\delta_{ij}(t-t')\ (j=1,2,3)$.

The corresponding moment equations by Gaussian closure procedure can be written as

$$\begin{cases}
\dot{m}_{100}=a(m_{010}-m_{100}),\\
\dot{m}_{010}=(c-a)m_{100}-m_{101}+cm_{010},\\
\dot{m}_{001}=m_{110}-bm_{001},\\
\dot{m}_{110}=(c-a)m_{200}+am_{020}+(c-a)m_{110}-(2m_{100}m_{101}+m_{200}m_{001}-2m_{100}^2m_{001}),\\
\dot{m}_{101}=a(m_{011}-m_{101})+(2m_{100}m_{110}+m_{200}m_{010}-2m_{100}^2m_{010})-bm_{101},\\
\dot{m}_{011}=(c-a)m_{101}-(2m_{001}m_{101}+m_{002}m_{100}-2m_{001}^2m_{100})+(c-b)m_{011}\\
\qquad\quad+(2m_{010}m_{110}+m_{020}m_{100}-2m_{010}^2m_{100}),\\
\dot{m}_{200}=2a(m_{110}-m_{200})+\sigma_2^2,\\
\dot{m}_{020}=2(c-a)m_{110}-2(m_{100}m_{011}+m_{010}m_{101}+m_{001}m_{110}-2m_{100}m_{010}m_{001})+2cm_{020}+\sigma_2^2,\\
\dot{m}_{002}=2(m_{100}m_{011}+m_{010}m_{101}+m_{001}m_{110}-2m_{100}m_{010}m_{001})+2bm_{002}+\sigma_3^2,
\end{cases} \tag{4.15}$$

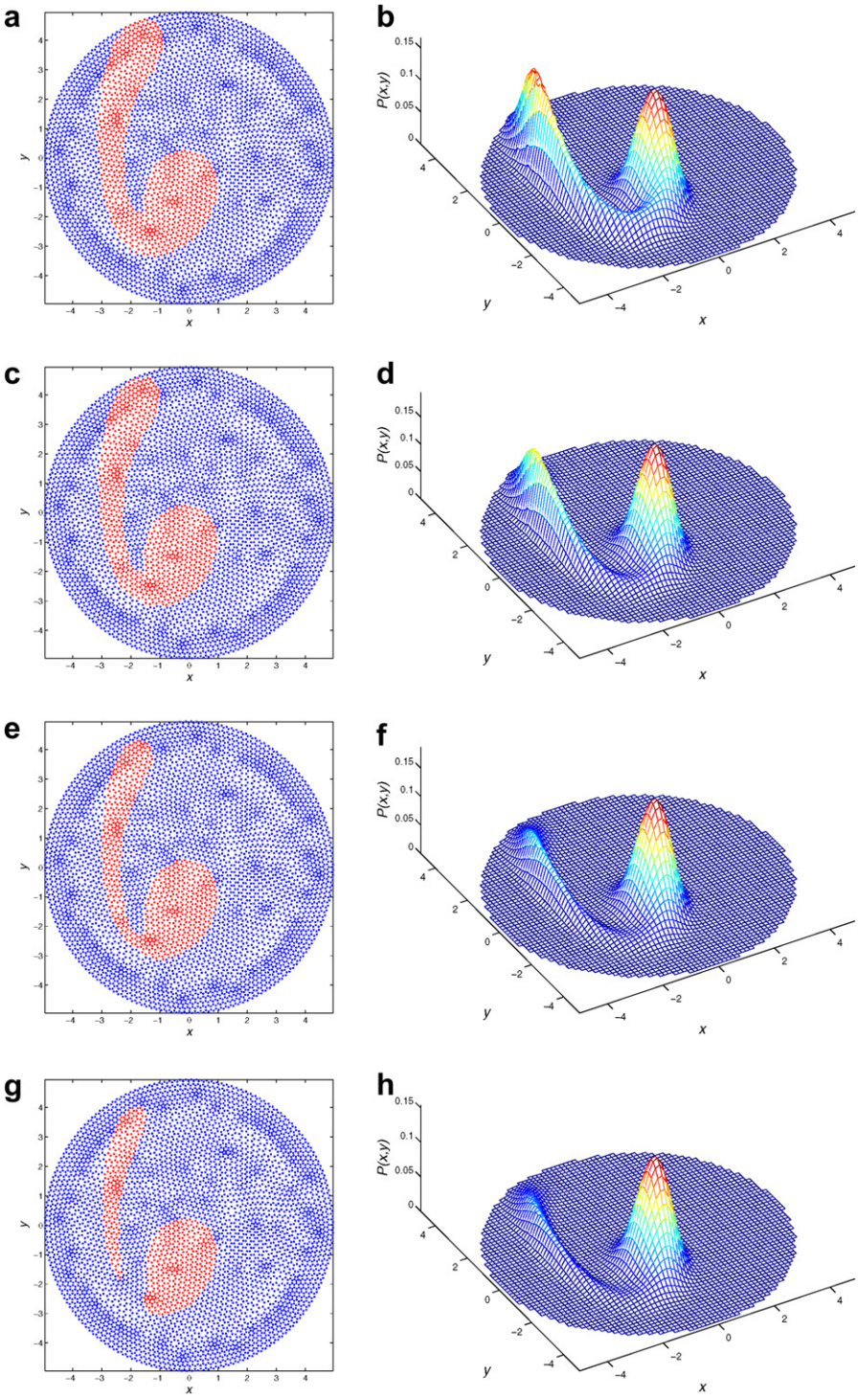

Fig. 3. Numerical results for Duffing–Rayleigh oscillator: (a) 2D plots at time $5T$: red nodes for $P(x,y) > 10^{-2}$, (b) surface plots at time $5T$, (c) 2D plots at time $25T$: red nodes for $P(x,y) > 10^{-2}$, (d) surface plots at time $25T$, (e) 2D plots at time $100T$: red nodes for $P(x,y) > 10^{-2}$, (f) surface plots at time $100T$, (g) 2D plots at time $200T$: red nodes for $P(x,y) > 10^{-2}$ and (h) surface plots at time $200T$. (For interpretation of the references to color in this figure legend, the reader is referred to the web version of this article.)

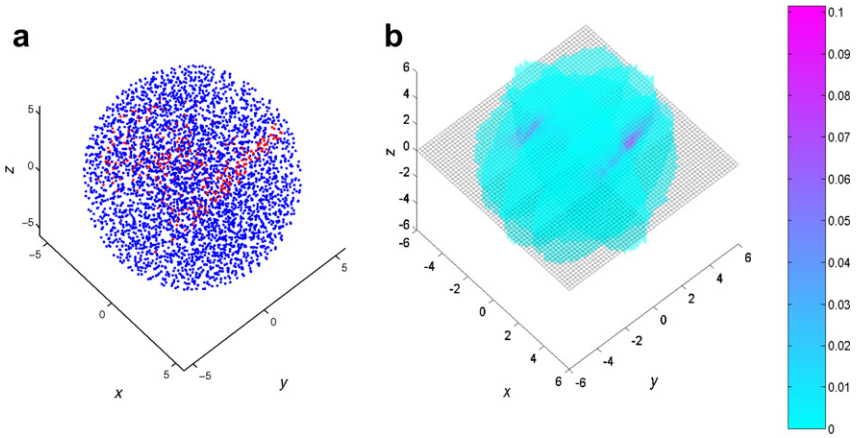

Fig. 4. Numerical result for CHEN system: (a) 3D plots at time 3π: red nodes for $P(x,y,z) > 10^{-3}$ and (b) volumetric slice plots at time 3π. (For interpretation of the references to color in this figure legend, the reader is referred to the web version of this article.)

where $m_{ijk} = E[x^i, y^j, z^k]$. Eqs. (4.15) are also solved numerically by the fourth-order NCERK method.

We can obtain the 3D transitional Gaussian distributions easily via Eq. (4.15) and our MPI method:

$$q(\mathbf{x}, t_n|\tilde{\mathbf{x}}, t_{n-1}) = \frac{1}{(2\pi)^{3/2}|\mathbf{B}(\tilde{\mathbf{x}}, t_n)|^{1/2}} \exp\left\{-\frac{1}{2}[\mathbf{x} - \mathbf{a}(\tilde{\mathbf{x}}, \mathbf{t_n})]^{\mathrm{T}}\mathbf{B}(\tilde{\mathbf{x}}, t_n)^{-1}[\mathbf{x} - \mathbf{a}(\tilde{\mathbf{x}}, \mathbf{t_n})]\right\}, \tag{4.16}$$

where $a_0 = [m_{100}(\tilde{\mathbf{x}}, t_n), m_{010}(\tilde{\mathbf{x}}, t_n), m_{001}(\tilde{\mathbf{x}}, t_n)]^{\mathrm{T}}$ and

$$\mathbf{B}(\tilde{\mathbf{x}}, t_n) = \begin{bmatrix} m_{200}(\tilde{\mathbf{x}}, t_n) - [m_{100}(\tilde{\mathbf{x}}, t_n)]^2 & m_{110}(\tilde{\mathbf{x}}, t_n) - m_{100}(\tilde{\mathbf{x}}, t_n)m_{010}(\tilde{\mathbf{x}}, t_n) & m_{101}(\tilde{\mathbf{x}}, t_n) - m_{100}(\tilde{\mathbf{x}}, t_n)m_{001}(\tilde{\mathbf{x}}, t_n) \\ m_{110}(\tilde{\mathbf{x}}, t_n) - m_{100}(\tilde{\mathbf{x}}, t_n)m_{010}(\tilde{\mathbf{x}}, t_n) & m_{020}(\tilde{\mathbf{x}}, t_n) - [m_{010}(\tilde{\mathbf{x}}, t_n)]^2 & m_{011}(\tilde{\mathbf{x}}, t_n) - m_{010}(\tilde{\mathbf{x}}, t_n)m_{001}(\tilde{\mathbf{x}}, t_n) \\ m_{101}(\tilde{\mathbf{x}}, t_n) - m_{100}(\tilde{\mathbf{x}}, t_n)m_{001}(\tilde{\mathbf{x}}, t_n) & m_{011}(\tilde{\mathbf{x}}, t_n) - m_{010}(\tilde{\mathbf{x}}, t_n)m_{001}(\tilde{\mathbf{x}}, t_n) & m_{002}(\tilde{\mathbf{x}}, t_n) - [m_{001}(\tilde{\mathbf{x}}, t_n)]^2 \end{bmatrix}.$$

There are 3907 nodes in the spheriform computational domain with the radius $r = 5.5$ and the time step Δt is π. The parameters of the initial Gaussian distribution are $\mu_1 = \mu_2 = \mu_3 = 0.0$, $s_1 = s_2 = s_3 = 1.0$ and $r_{12} = r_{13} = r_{23} = 0.0$. We choose $a = 0.5$, $b = 2.72$, $c = 1.0$, $\sigma_1 = \sigma_2 = 0.0$ and $\sigma_3 = 0.8$. Fig. 4 offers the numerical probability density at time 3π. Two steady state points of the CHEN system can be observed clearly in the probability density, see Fig. 4.

5. Conclusions

We present a new numerical path integration method, i.e., MPI method, for non-linear dynamic systems. The obtained MPI method can be performed in the irregular computational domain and the probability density values of the random nodes in the domain can be easily calculated. Three experiments are solved successfully and the efficiency of the methodology is verified. Simultaneously, some smart dynamical behaviors of the Duffing oscillator, Duffing–Rayleigh oscillator and CHEN system are also described herein.

Acknowledgements

The authors gratefully acknowledge the support of Youth for Northwestern Polytechnical University Teachers Scientific and Technological Innovation Foundation.

References

[1] H. Risken, The Fokker–Planck Equation, Springer-Verlag, 1989.
[2] M.F. Wehner, W.G. Wolfer, Numerical evaluation of path-integral solutions to Fokker–Planck equations, Physical Review A 27 (5) (1983) 2663–2670.

[3] M.F. Wehner, W.G. Wolfer, Numerical evaluation of path-integral solutions to Fokker–Planck equations II, restricted stochastic processes, Physical Review A 28 (5) (1983) 3003–3011.
[4] M.F. Wehner, W.G. Wolfer, Numerical evaluation of path-integral solutions to Fokker–Planck equations III, time and functionally dependent coefficients, Physical Review A 35 (4) (1987) 1795–1801.
[5] A. Naess, J.M. Johnsen, Response statistics of nonlinear compliant structures by the path integral solution method, Probabilistic Engineering Mechanics 8 (1993) 91–106.
[6] A. Naess, V. Moe, Stationary and non-stationary random vibration of oscillators with bilinear hysteresis, International Journal of Non-Linear Mechanics 31 (5) (1996) 553–562.
[7] A. Naess, IASSAR report on computational stochastic mechanics, Probabilistic Engineering Mechanics 12 (1997) 257–260.
[8] A. Naess, V. Moe, Efficient path integration methods for nonlinear dynamic systems, Probabilistic Engineering Mechanics 15 (2000) 221–231.
[9] J.S. Yu, G.Q. Cai, Y.K. Lin, A new path procedure based on Gauss–Legendre scheme, International Journal of Non-Linear Mechanics 32 (4) (1997) 759–768.
[10] J.S. Yu, Y.K. Lin, Numerical path integration of a non-homogeneous Markov process, International Journal of Non-Linear Mechanics 39 (2004) 1493–1500.
[11] K. Sobczyk, J. Trebicki, Approximate probability distributions for stochastic systems: maximum entropy method, Computer Methods in Applied Mechanics and Engineering 168 (1999) 91–111.
[12] W.X. Xie, W. Xu, L. Cai, Path intergration of the Duffing–Rayleigh oscillator subject to harmonic and stochastic excitations, Applied Mathematics and Computation 171 (2005) 870–884.
[13] W.X. Xie, W. Xu, L. Cai, Study of the Duffing–Rayleigh oscillator subject to harmonic and stochastic excitations by path integration, Applied Mathematics and Computation 172 (2006) 1212–1224.
[14] W.X. Xie, L. Cai, J.H. Feng, W. Xu, Computations of shallow water equation with high-order central-upwind schemes on triangular meshes, Applied Mathematics and Computation 170 (2005) 296–313.
[15] M. Zennaro, Natural continuous extensions of Runge–Kutta methods, Mathematics of Computation 46 (1986) 119–133.
[16] J.H. Lü, T.S. Zhou, G.R. Chen, S.C. Zhang, Local bifurcations of the CHEN system, International Journal of Bifurcation and Chaos 12 (10) (2002) 2257–2270.
[17] J.H. Lü, G.R. Chen, D.Z. Cheng, S. Celikovsky, Bridge the gap between the Lorenz system and the CHEN system, International Journal of Bifurcation and Chaos 12 (12) (2002) 2917–2926.